# Improving the Estimation of Soil Moisture in Semi-Arid Regions Using Data from Different Remote Sensing Techniques

**Youssef, N. M.,[1,2] Gad, M. A.,[1]* Elmoustafa, A. M.[1] and Elleithy, D.[1]**
[1]Irrigation and Hydraulics Department, Faculty of Engineering, Ain Shams University, Egypt
E-mails: eng_nohayoussef@yahoo.com, hydroshams@yahoo.ca,* ashraf_elmoustafa@eng.asu.edu.eg, dina.elleithy@eng.asu.edu.eg
[2]Water Resources Research Institute, National Water Research Center, Egypt
*Corresponding Author*

**DOI: https://doi.org/10.52939/ijg.v19i8.2781**

**Abstract**
*Satellite-derived soil moisture fields received attention due to their large spatial coverage and spatial resolution that suits many applications. The sensors used vary from passive (e.g., LANDSAT-8) to active (e.g., SENTINEL-1) with varying accuracy problems. Passive sensing can only determine relative indices between pixels within a vegetation class and not the real value of moisture. Active sensing suffers from the sensitivity of its detecting behaviour to the level of moisture (anomalous backscatter). The above problems impose limitations on the application without frequent ground-based calibration. The paper investigates possible models to improve the estimation of soil moisture using the powers of the two sensors. In addition, a Hydrologic Surface Moisture indicator (HSM) is included as a third source of information. The paper tests modeling combinations of the three soil moisture predictors (Landsat-8, Sentinel-1, and HSM). The models are validated using in-situ measurements. The results showed that Landsat-8 data can be rescaled using HSM to provide the actual soil moisture in the soil. On the other side, it is possible to remove the anomaly from the Sentinel-1 backscatter using either Landsat-8 or HSM. The elimination of the above problems explained a significant portion of the differences between the two sensors.*

**Keywords:** Anomalous, Hydrologic, Landsat-8, Sentinel-1, Soil Moisture

## 1. Introduction

Soil moisture has been conventionally measured using observing equipment such as time-domain reflectometry (TDR), which provides a few quantities of point data. This method has limitations in representing soil moisture for a wide area with spatially variable characteristics. The improvements in remote sensing technology in terms of high efficiency, low cost, real-time, and wide spatial coverage [1] attracted researchers to use these products. Direct and indirect methods of detecting soil moisture content (SMC) are utilized in remote sensing.The indirect method (i.e., the passive method) is using passive satellite-born thermal camera (e.g., Landsat-8), where an indication of the spatial variability of moisture can be determined as a function in both LST (Land Surface Temperature) and NDVI (Normalized Difference Vegetation Index). The spatial variability of moisture is expressed in terms of the soil moisture index (SMI) which represents the moisture relative to other pixels in the same vegetation class (in the same image). SMI can be simply determined by relating the LST of a pixel to the minimum and maximum LST in the same vegetation/image [2] [3] [4] [5] and [6]. Zero SMI indicates the least moisture in the same NDVI/image while 1 indicates the maximum moisture relatively. The value of SMI cannot tell dry or wet, rather it gives a figure of how moist a pixel is in relation to its neighbourhood in the same NDVI /image. Hence, the actual moisture pixel values cannot be determined unless the image is calibrated by known actual soil moisture content (SMC) in one or more pixels in the same NDVI /image. The direct method (i.e., the active method) employs an active radar sensor on board the satellites [**7**]. This makes the detection more related to SMC (since the detection is direct). The active method (e.g., Sentinel-1) calculates SMC based on the backscattered energy to the radar antenna that is affected by the surface soil moisture.

Microwave frequencies in the C-band are good for estimating soil moisture compared to other spectral bands [8]. The C-band has an advantage that it can penetrate clouds as opposed to the passive sensors that fail to provide continuous monitoring in cases of cloud existence. For the above reasons (accuracy and continuity), the use of active microwave remote sensing in detecting soil moisture became a recent active research topic [9] [10] [11] [12] [13] and [14]. Backscatter represents the portion of the emitted radar signal that the target returns towards the radar antenna, it was commonly represented in remote sensing by the sigma symbol $\sigma_o$ (i.e., the backscattering coefficient) expressed in decibels (dB). Theoretically, the backscattered energy should be directly related to the soil moisture content SMC for the same acquisition geometrical conditions (should increase together) [15] and [16].

However, in cases of anomalous backscattering, the situation reverses. The anomalous backscattering has been repeatedly reported in many studies in the literature [17]. In Europe, some researchers have attributed this to the contribution of the subsurface in a dry condition which leads to an anomalous turning point in soil moisture below which an anomalous increase in backscattering occurs [17] [18] [19] and [20]. The situation becomes more complicated in semi-arid regions (e.g., North Africa) where there is another turning point in soil moisture above which an anomalous decrease in backscattering also occurs [see the North African sites in [17].

Certainly, the semi-arid case cannot be attributed to the subsurface backscattering since this is a wet condition. The semi-arid anomaly is yet not explained in the literature, which constitutes a gap in research. What is important to note here is that both anomalies, even though they are at two different turning points (moisture-wise); but they are both related to the level of moisture in the soil. Hence, an additional source of information (with Sentinel-1) regarding the level of moisture in the soil can assist in detecting on which side of these two turning points Sentinel-1 data at a certain area falls. The paper investigates two possible sources of this additional information (Landsat-8 or a hydrologic indicator). It is important to mention also that Landsat-8, luckily, does not suffer from this anomaly. The paper also tests possible improvements on Landsat-8 using this hydrologic indicator. Hence, the combinations between the three predictors (Landsat-8, Sentinel-1, and a Hydrologic Indicator) are investigated in this research in a trial to reach a better soil moisture estimation.

## 2. Study Area

The North Coast region of Egypt is distinguished by heavy rainfall through the rainy season from September to April with an average annual rainfall varying between 100 mm and 190 mm [21]. The dry season (May to August) is associated with zero rainfall. The daily rainfall data are available from 2015 to 2023 at Matrouh rain gauge shown in Figure 1. The weather belongs to the south Mediterranean area where the minimum and maximum temperatures in Matrouh station vary between lowest values in January (min= 7°C and max = 20 °C) to its highest values in June (min. = 17°C and max. = 37°C). Sparse Rain-fed crops and trees (olive and fig) are the traditional agricultural crops in the North Western Coast of Egypt depending on winter rainfall. This is usually executed in flat Wadi areas (represented by the study area) where a collection/diversion of small earth dikes are sometimes used to harvest floodwaters. The study area is located near Matrouh City at a longitude 27.2° and latitude 31.29° (refer to Figure 1). The soil type, on average, is sandy clay loam. However, the percentage of clay/sand significantly differs from one location to another, according to laboratory results. A large number of in-situ SMC measurements were carried out along the Wadi in the study area (100 measurements divided into 5 different datasets as described in the next section below).

## 3. Data Processing

The datasets consist of in-situ SMC (Soil Moisture Content) measurements taken at five different dates as well as the corresponding remote sensing data from Landsat-8 and Sentinel-1. Table 1 shows the measurement and acquisition dates of the data.

### *3.1 In-situ Measurements*

Five datasets with one hundred total readings of SMC % were performed at selected twenty locations along the Wadi (Figure 1) shows the measurements locations. The 100 readings are distributed on the 5 different dates given in Figure 2 (20 readings per dataset). The soil moisture content readings in dataset no. 3 in Figure 2 and Table 1 were taken from the literature [22]. The soil moisture measurements in the remaining 4 datasets were performed by the research team using ML2X Theta Probe (Figure 3) to measure the soil moisture content (SMC) in the soil within a depth that varies from 5 to 10 cm. Theta Probe measures volumetric soil moisture content within ±1% or ± 0.01 $m^3.m^{-3}$ accuracy.

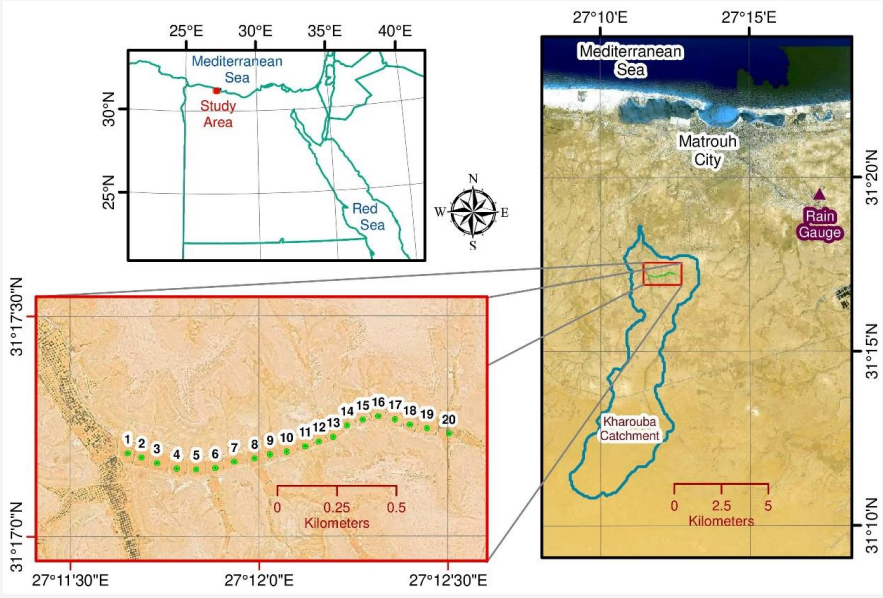


**Figure 1:** Location map of the study area. Spatial coverage and sampling locations of Soil moisture content measurements at 20 sites along the Wadi for five different dates

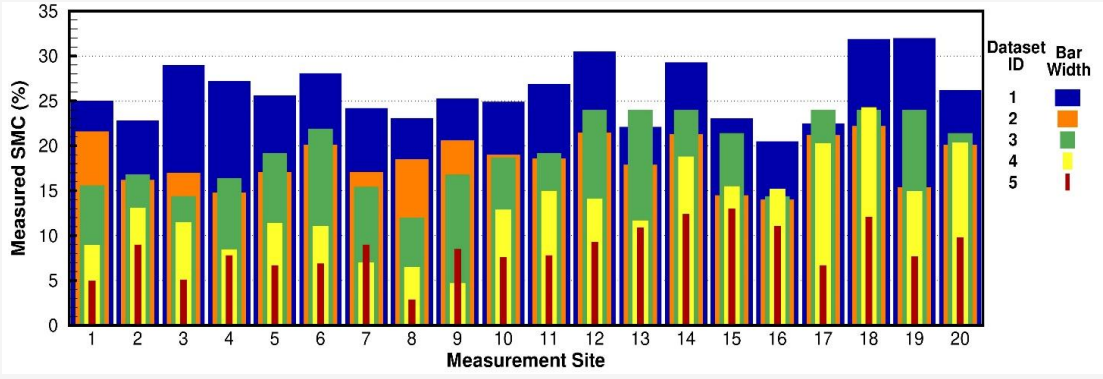


**Figure 2:** Soil Moisture Content (SMC) readings measured using ML2X Theta probe in the five different datasets shown in Table (1). The datasets are given IDs from 1 to 5 in descending order from wet to dry (refer to Table 1). Each one of the 5 datasets is composed of 20 readings (at the 20 measuring locations shown in Figure 1). Readings of dataset no.3 were taken from [22] and the other four datasets are new in-situ measurements

**Figure 2:** Soil Moisture Content (SMC) in-situ measurements. The left panel shows a photo of the Wadi where the 20 measuring locations exist and the right panel was taken during a measurement

**Table 1:** Details of the five selected datasets

| ID | Status | Dataset Time Frame | | | *Rainfall during the Dataset Time Frame | **HSM% |
|---|---|---|---|---|---|---|
| | | In-Situ Measurements Date | Landsat-8 Acquisition Date | Sentinel-1 Acquisition Date | | |
| 1 | Wet | 6 Feb. 2022 | 6 Feb. 2022 | 11 Feb. 2022 | 0 | 53.2 |
| 2 | Wet | 1 Dec. 2021 | **NA | 1 Dec. 2021 | 0 | 45.1 |
| 3 | Wet | 16 Jan. 2016 | 21 Jan. 2016 | 18 Jan. 2016 | 0 | 18.9 |
| 4 | Dry | 17 Mar. 2022 | **NA | 19 Mar. 2022 | 0 | 5.6 |
| 5 | Dry | 10 Nov. 2021 | 02 Nov. 2021 | 11 Nov. 2021 | 0 | 4.0 |

**No rainfall occurred during the dataset time frame*
***HSM is the Hydrologic Surface Moisture Indicator (refer to section 3.4)*
***NA: Landsat-8 data is not available due to clouds existence*

Volumetric soil moisture content is the ratio between the volume of water present to the total volume of the sample. This is a dimensionless parameter, expressed as either a percentage or a ratio. Full details are available in the ML2X Theta probe manual at: *https://www.labima.unifi.it/upload/sub/Strumentazione/Manuali/ML2x%20ThetaProbe%20User%20Manual%20v1.21.pdf*.

Table 1 shows the datasets measurements and acquisition time frame (i.e., dates of the in-situ measurements as well as the acquisition dates of Landsat-8 and Sentinel-1). Note that the datasets shown in Table 1 are ranked from wet to dry. The two datasets no. 4 and 5 (i.e., the fourth and fifth) in Table 1 are associated with relatively dry cases while the remaining 3 datasets (the first, second, and third) are relatively wet cases with the maximum SMC values measured in dataset no.1 (i.e., Feb. 2022). Note that the measuring and acquisition dates are slightly different due to the different revisit times of Landsat-8 and Sentinel-1. Hence, for comparison reasons, it is important to check that no rainfall occurred between dates to ensure that there is no sudden change in soil moisture that can create discrepancies between the three sources of soil moisture (i.e., measured, Landsat-8, and Sentinel-1). Therefore, the rainfall data at Matrouh rain gauge (shown in Figures 5 and 6) are used to perform this check (i.e., ensuring zero rainfall between dates).

*3.2 Landsat-8 Data (SMI)*

The USGS website https://earthexplorer.usgs.gov/ was used to download the data of Landsat-8 represented in the two sensors (OLI/TIRS). The study area's location was specified by defining the Path and Row of the region, and the data were collected throughout the selected dates. The spatial resolution of downloaded TIRS (Thermal Infrared Sensor) images of Landsat-8 is 30 m (resampled from 100 m using cubic convolution). SMI was calculated in terms of the land surface temperature only since the area has the same vegetation class. The calculation method is described in [23]. Thermal and radiometric corrections were considered during the processing of Landsat - 8 data using ENVI 5.3 software to estimate LST [24]. Since the whole North Western Coast of Egypt (including the study area) falls into one vegetation class, only LST is used (i.e., NDVI is excluded) to develop the standard Soil Moisture index, an LST image (i.e., raster or grid) is converted to standard SMI grid, using GIS raster calculations, using the standard relative moisture in Equation 1 as follows:

$$SMI_i = \frac{LST_{max} - LST_i}{LST_{max} - LST_{min}}$$

Equation 1

Where:

$SMI_i$ = Standard Soil Moisture Index at pixel *i* of a grid
$LST_i$ = Land Surface Temperature at pixel *i* of the grid
$LST_{max}$ = Maximum Land Surface Temperature inside the grid
$LST_{min}$ = Minimum Land Surface Temperature inside the grid

GIS is then used to extract SMI values at the 20 locations on 3 different cloud-free dates (Jan. 2016, Nov.2021, and Feb.2022). The extracted values are shown in Figure (4a). Note also that the shown SMI values are not comparable between the three datasets, since they are relative values in each date (refer to the introduction section).

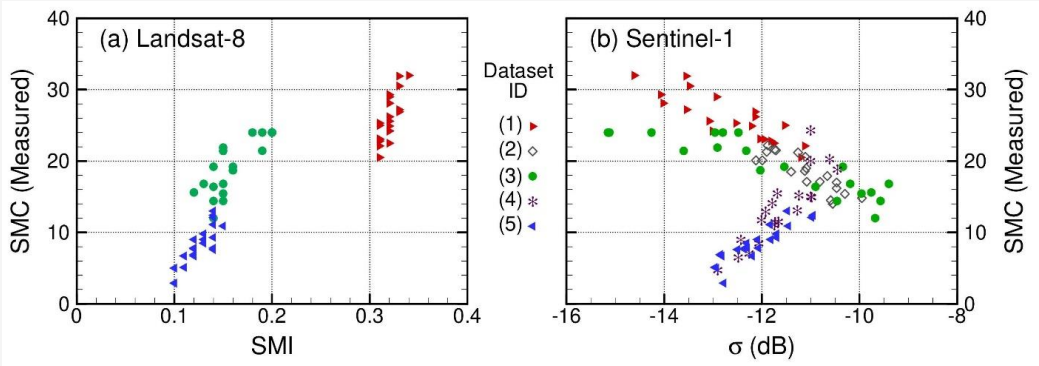


**Figure 4:** Pre-processed remote sensing data extracted at the 20 sites for the different datasets. (a) Landsat-8 and (b) Sentinel-1 σo (referred to as σ only for symbolization simplicity). Note that 3 datasets are only considered for Landsat-8 (cloud-free)

*3.3 Sentinel-1 Data ($\sigma_o$, Referred to as σ)*

Sentinel-1 satellites (A and B) were launched in April 2014 and 2016 with the same orbital plane. The radar is a Synthetic Aperture Radar (SAR) C-band with a frequency of 5.405 GHz [25]. An image of nearly 10 m horizontal resolution (in Level0 and Level1 data processing) is available with a repeat cycle of 12 days for each satellite. When both satellites are used together, the cycle can be reduced to 6 days. However, care should be taken in comparing the data from A and B due to the different viewing angles of the same point on Earth from A and B. This can be problematic (even with corrections) in cases of mountainous slopes that can dramatically change the incident angle.

Sentinel-1A data were downloaded for 5 dates from Copernicus website https://scihub.copernicus.eu/dhus/#/home. The data are Level-1 Ground Range Detected (GRD-level-1) products with VV and VH polarization. The spatial resolution is 10 m. Only VV polarization was processed due to the weak correlation between soil moisture and VH polarization [13] and [3]. The backscattering coefficient (σ) was estimated in decibels units (dB) using Sentinel Application Platform (SNAP) software. Note that σ is referred to σ (without the nought symbol) in this paper for simplicity of the symbolization in the equations. SNAP pre-processing involves noise removal (border and thermal), radiometric calibration, speckle filtering, terrain correction, and logarithmic conversion to decibels (dB). The methodology for Sentinel-1 data pre-processing is described in [26], additional literature can be found in [3] and [27]. Figure 4(b) presents the backscattering coefficient for the five datasets.

*3.4 Rain Gauge Data (HSM)*

The Egyptian Water Resources Research Institute (WRRI) operates a tipping bucket rain gauge near the study area (refer back to Figure 1). Rainfall data were obtained from the gauge logger and accumulated on daily intervals to provide a day-by-day independent indication of the soil moisture condition (i.e., independent of the remote sensing data).

A simplified procedure is developed to calculate a hydrologic indicator for the level of surface moisture. The indicator is called the Hydrologic Surface Moisture (*HSM*). It is a function in the Total Infiltrated Precipitation (*TIP*) from the last 30 days' precipitation records assuming exponential decay over time from each day, with linear adjustment due to evaporation. The procedure follows the Curve Number SCS method (Soil Conservation Method) infiltration model [28] with a slight modification to include a time decay function and evaporation adjustment. In other words, *TIP* is assumed to be the linear superposition of the effects of each of the previous 30 days (including zero records). The far precipitation occurs back in time from the date of interest, the less weight it takes in the summation at this date of interest. To illustrate the procedure, let $CN_{dry}$ and $CN_{wet}$ denote rough estimates for the curve number for the dry and wet cases. The curve number at any day $t$ can be found according to the total precipitation in the previous 5 days ($P_{5d(t)}$ in mm units) as follows in Equation 2 (refer to [28] for the details of the standard SCS method):

$$CN_t = \begin{cases} CN_{dry} & \left(If\ P_{5d(t)} = 0mm\right) \\ CN_{wet} & \left(If\ P_{5d(t)} \geq 15mm\right) \\ CN_{dry} + \mathrm{P}_{5d\,(t)} \dfrac{CN_{Wet} - CN_{dry}}{15} & (Else) \end{cases}$$

Equation 2

The underneath maximum soil potential storage at this day ($S_t$) in (mm) is calculated according to the SCS method as expressed in Equation 3:

$$S_t = \frac{25400}{CN_t} - 254$$

Equation 3

Let the daily precipitation depth during this day only be $P_t$, the infiltrated precipitation (*IP* in mm) during this day only can be estimated from the SCS standard equation (Equation 4):

$$IP_t = \begin{cases} P_t - \dfrac{(P_t - 0.2S_t)^2}{P_t + 0.8S_t} & (If\ P_t > 0.2S_t) \\ P_t & (Else) \end{cases}$$

Equation 4

In order to get the total infiltrated precipitation (*TIP*) at a time (*t*) in mm, the effects of the previous 30 days are added using exponential decay with linear weighting as shown in Equation 5:

$$TIP_t = \sum_{n=1}^{n=30} k_2 \times IP_{t-n} \times e^{-k_1 n}$$

Equation 5

Where $k_1$ is the exponential decay coefficient (taken as 0.125 in this study) and $k_2$ is the evaporation scaler taken as 1, 0.9, 0.6, 0.5, 0.4, 0.4, 0.4, 0.4, 0.5, 0.6, 0.7, 0.85 for months from January to December. Finally, a rough estimate of the Hydrologic Surface Moisture (*HSM*) at a time (*t)* is obtained as a percentage by dividing $TIP_t$ by the dry initial abstraction ($0.2S_d$) as follows (Equations 6 and 7):

$$HSM_t = \frac{TIP_t}{0.2 \times S_d} \times 100 \qquad (\leq 100)$$

Equation 6

Where:

$$S_d = \frac{25400}{CN_d} - 254$$

Equation 7

Note that the procedure above considers only the rainfall infiltrated into the soil and the excess rainfall (i.e., runoff) is ruled out. A value of $CN_{dry}$ = 75 and $CN_{wet}$ = 85 are used in the calculations since these are the typical values for the soil in the semi-arid Egyptian North Western Coast [29] [30] and [31]. Figure 5 presents the daily rainfall hyetograph and the daily calculated HSM during the period 2015-2022 using the daily precipitation data. The temporal positions of the five datasets considered in this study are shown on the timeline (x-axis) on the figure using vertical dotted lines. HSM values of the five datasets are also shown in Table 1. These five HSM values can be used as a rough indicator in the modeling section below. Figure 6 zooms to the period from October 2021 to April 2022 to demonstrate the functionality of the pre-processing methodology.

It should be noted that the results in the modeling section below are not sensitive to the values of the parameters used in HSM calculations (i.e., $CN_{dry}$, $CN_{wet}$, $k_1$ and $k_2$) as long as model coefficients in the next section are obtained through calibration using SMC data. In other words, model coefficients (next section) are already obtained using the chosen values above.

## 4. SMC Modelling

### *4.1 One Predictor Model (SMI or σ)*

Since Landsat-8 can measure only the spatial variability of moisture in a spatially relative sense in each image (refer back to the introduction section), it is not possible to use Landsat-8 alone to model SMC without sufficient ground-based calibration. The problem is that ground-based calibration is actually needed for each image and model coefficients calibrated for a certain image cannot be generalized between images at different dates unless the meteorological conditions are the same. This is because LSTs (land Surface Temperatures) not only function in soil moisture alone, but they also function in other meteorological variables. For example, the SMI values plotted in Figure 4(a) can only be used for the same dates to judge relative variation in the same image but cannot be used to judge moisture change across dates since each date has completely different LSTs and equation 1 only scales the SMI across the same image (and not across images).

On the other side, Sentinel-1 backscattering has the advantage of being related to SMC in an absolute sense (i.e., model coefficients, if calibrated once, can be generalized across dates). However, although Sentinel-1 is more precise in detecting soil moisture (active-based), the situation becomes more complicated here actually since the scattering behaviour suffers anomalous backscattering (refer to the introduction and the discussion sections). In other words, a certain value of backscattering may pertain to two different σ-SMC relations (the normal or the anomalous). For example, the backscattering behaviour shown in Figure 4(b) completely and anomalously reverses in wet conditions. Hence, for a certain backscattering value on the x-axis, there are two SMC solutions on the y-axis for the normal and reversed legs.

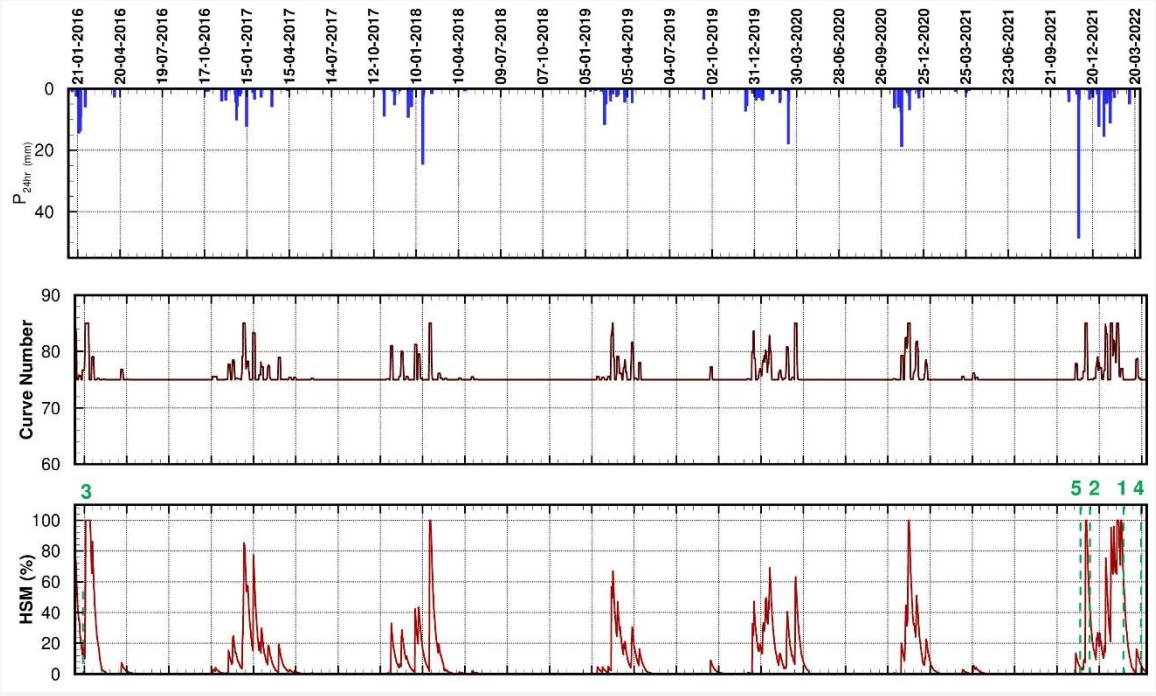


**Figure 5:** Time series of daily precipitation (upper panel), Curve Number (middle), and HSM (bottom) from Jan. 2015 to April 2022 (positions of the 5 datasets are shown by dotted lines)

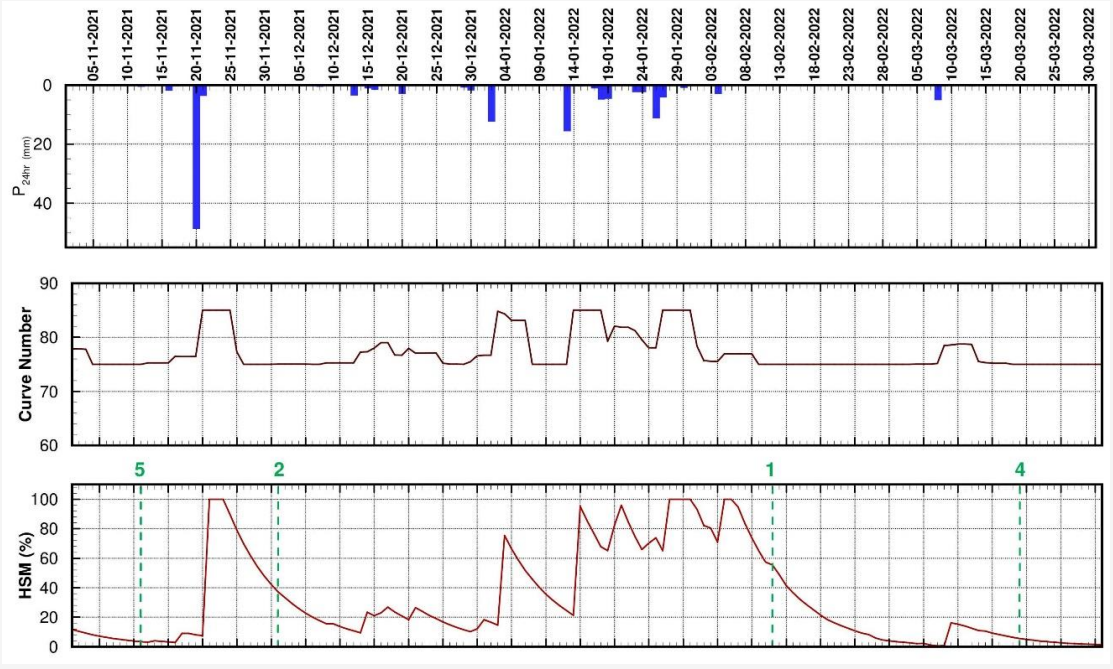


**Figure 6:** Time series of daily precipitation (upper panel), Curve Number (middle), and HSM (bottom) during the rainy season of Oct. 2021 to March 2022 (positions of 4 datasets are shown by dotted lines)

To solve the problem, another source of information is needed to tell which leg of the relation to use. This may require calibration of every image using ground-based measurement (which is not feasible since it takes away the reliable strength of Sentinel-1 of being direct). Hence, it can be concluded that a single predictor model (whether it is Landsat-8 alone or Sentinel-1 alone) is not possible and an additional second predictor is essential for this case study.

*4.2 Two Predictors (SMI & HSM)*

The idea here is to re-scale the image-specific relative SMI using HSM as an absolute soil moisture scaler. This can move the SMI from the relative scale to the absolute scale. In other words, HSM can be seen as a calibration point corresponding to the average of Landsat-8 pixels that falls under this value of *HSM* (i.e., covered under this rain gauge umbrella or rainfall bigger pixel if gridded precipitation is used). To explain this type of SMI-SMC model, let $SSMI_i$ denotes the "Scaled" Soil Moisture Index for pixel *i* at a certain date that can be calculated from Equation 8:

$$SSMI_i = \frac{SMI_i}{SMI_{av}} \quad \text{Equation 8}$$

Where:

$SMI_i$ = Standard Soil Moisture Index (Equation 1)

$SMI_{av}$ = Average SMI under the rain gauge umbrella = $\frac{1}{n}\sum_{i=1}^{i=n}(SMI_i)$

$n$ = Number of pixels under the rain\ gauge umbrella

The SMC model can then be expressed as follows (Equation 9):

$$SMC_{model,i} = a_{HSM}\left(SSMI_i\right) \quad \text{Equation 9}$$

Where:

$$a_{HSM} = a_1 + b_1\, Ln\left(HSM + 1\right) \quad \text{Equation 10}$$

The optimum model coefficients of the above model ($a_1$, and $b_1$) are obtained by minimizing the Sum Square of Errors (SSE) between the model and in-situ SMC readings in the 3 cloud-free datasets as shown in Equation 11:

$$SSE = \sum\left(SMC_{modeled} - SMC_{observed}\right)^2 \quad \text{Equation 11}$$

The optimum values are $a_1$ = 2 and $b_1$ = 6.1. Note that these values are supposed to be general and are usable across dates. Figure 7(a) compares the observed to the modeled SMC using the optimum coefficients. The value of 1 in Equation 10 is used to eliminate logarithm zero (it is merely a representation of the dry hygroscopic water).

*4.3 Two Predictors (σ & HSM)*

Here the observed SMC is regressed to both Sentinel1-σ and HSM using a composite 4 coefficients model. The idea here is also that *SMC* is linearly related to σ. The coefficients of the linear model ($a_{HSM}$ & $b_{HSM}$) are nonlinearly related to *HSM*. This allows for scaling the linear relation according to the level of surface moisture (*HSM*). In other words, the model considers that the linear relation is a function in the moisture case (refer to Figure 4(b) to compare between datasets). Hence, let $\sigma_i$ denotes the backscatter at pixel *i* under the rain gauge umbrella (or under a rainfall pixel in grid-based rainfall products), hence, the modeled *SMC* at pixel *i* is expressed as follows:

$$SMC_{model,i} = a_{HSM} + (b_{HSM})\sigma_i \quad \text{Equation 12}$$

Where:

$$a_{HSM} = a_2 + b_2\,\mathrm{Ln}\left(HSM + 1\right) \quad \text{Equation 13}$$

$$b_{HSM} = a_3 + b_3\,\mathrm{Ln}\left(HSM + 1\right) \quad \text{Equation 14}$$

The optimum model coefficients are obtained by minimizing the sum square of errors (*SSE*) between the model and observations (in the 5 datasets) similar to the previous section. The optimum values for the four coefficients are $a_2$ = 9, $b_2$ = -3.2, $a_3$ = 111, & $b_3$= -33.4. Figure 7(b) plots the modeled *SMC* to the observed *SMC*. Note that these two predictors-models significantly explained the relation between the backscattering coefficient and the in-situ SMC readings. In addition, it could also explain the anomalous backscattering behaviour.

*4.4 Two Predictors (σ & SMI)*

Here, a correlation-based technique is developed. The main idea is to use Landsat-8 data to identify anomalous behaviour in Sentinel-1. First, two fixed linear models are fitted to simulate the normal and the anomalous conditions in Sentinel-1 backscatter (the increasing and the revered legs in Figure 4(b) as shown in Equations 15 and 16:

$$SMC_{model,i}\left(normal\right) = 81.8 + 6\sigma_i \quad \text{Equation 15}$$

$$SMC_{model,i}\left(anomolous\right) = -11.8 - 2.8\sigma_i \quad \text{Equation 16}$$

To decide which model to be used, the two images (i.e., Landsat-8 and Sentinel1-) corresponding to the same dataset are clipped to the Wadi area (correlation area) and then spatially cross-correlated as follows (Equation 17):

$$\rho = \frac{\frac{1}{N}\sum_{i=1}^{i=N}\left(SMI_i - SMI_{av}\right)\left(\sigma_i - \sigma_{av}\right)}{STDEV_{SMI} \times STDEV_{\sigma}}$$

Equation 17

Where:

$\rho$ = the cross-correlation coefficient
$SMI_i$ = Soil Moisture index from Landsat-8 at pixel *i*.
$\sigma_i$ = Backscattering coefficient from Sentinel-1 at pixel *i*.
$SMI_{av}$ & $\sigma_{av}$ = Averages of *SMI* and $\sigma$ respectively over *N* pixels
*STDEV* = Standard deviation of a variable (the subscript symbol) over *N* pixels
*N* = Number of pixels in the correlation area (i.e., Wadi area)

Hence, for a positive cross-correlation value for the study area, equation (15) is used, and for a negative value, Equation (16) is used. Figure 7(c) compares the modeled and observed SMC for the 3 cloud-free events. The plot shows that the use of Landsat-8 as an anomaly indicator is a very good idea that can solve the anomalous backscattering issue.

## 5. Conclusions and Discussion

The paper tests 3 modeling approaches using 2 predictors: Landsat-8 with HSM, Sentinel-1 with HSM, and Sentinel-1 with Landsat-8 for soil moisture estimation. The reason for using two-predictors is to overcome the problems involved in the one predictor approaches discussed in the paper. It is worth highlighting some points regarding the sources of errors (i.e., limitations) that can affect the accuracy of the three modeling approaches. For that reason, it is beneficial to discuss first some important acquisition errors. This is because acquisition errors are automatically inherited in any modeling approaches. For example, Landsat-8 surface temperatures can be sensitive to cloud interference or significant differences in elevation (due to the lapse rate that can cause cooling of the land surface). Another example of acquisition errors is the sensitivity of Sentinel-1 to big changes of the beam incident angle due to hill slopes, which limits the successful application to the relatively flat areas. On the other side, rainfall measurements (used to estimate HSM) can contain different errors. For example, tipping bucket gauges are point measurements and not spatially continuous gridded precipitation; they can also suffer errors due to disturbance, partial blockage, or major total absence of tips. In case gridded rainfall products are used (e.g., weather radars), there are other sources of errors that can be involved in measuring rainfall.

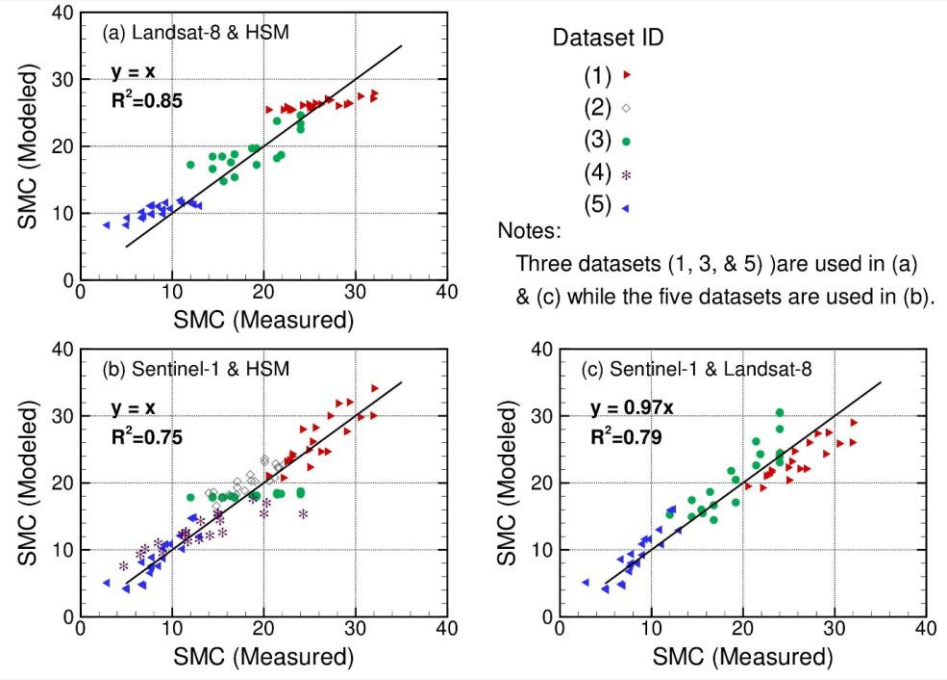


**Figure 7:** Modelled SMC using the three different two-predictor models (sections 4.2, 4.3 and 4.4)

Accordingly, taking the above sources of errors into consideration; the accuracy-related limitations (as well as the advantages) of the three modeling approaches can be summarized as follows:

- The first approach (Landsat-8 with HSM) could transfer Landsat-8 image-relative indices to be absolutes soil moisture values. This means that Landsat-8 data can now be applied across images (i.e., across dates) using this approach. However, this approach is dependent on the HSM values as HSM is used to scale SMI. Accordingly, it is calibration demanding (requires frequent calibration) as well as error-free rainfall (and/or irrigation) data. Although, the $R^2$ value of this approach is slightly higher in the paper, but it cannot be said that this approach is more practical for the above reasons in addition to the cloud free requirements of using Landsat-8. Moreover, only 3 datasets (three cloud-free dates only) in the paper are used for assessment.
- The second approach (Sentinel-1 with HSM) inherits the power of Sentinel-1 as a radar direct soil moisture detector. The approach requires relatively less calibration since it is direct measurements. However, it is still dependent on HSM that requires error free rainfall data (and/or irrigation data). It should be noted that the assessment of this approach in the paper is based on 5 datasets (not 3 as in the other two approaches) which gives rise to more confidence in its performance.
- The third approach (Sentinel-1 with Landsat-8) seems the simplest and most efficient approach since it blends the powers of the two sensors (i.e., Sentinel-1 and Landsat-8). Here Landsat-8 only acts as an anomaly detector for Sentinel-1 and not as a scaler. Hence, the technique requires the least calibration since Sentinel-1 only is involved in the calibration. However, the most important source of problems is the difference in the revisit times of the two satellites. Hence, the approach is only applicable in cases when no rainfall (or irrigation) occurs between the revisit times of the two satellites. In addition, and of course, the technique is only applicable in cloud free cases (due to Landsat-8). It should be noted here that the above two limitations of this third approach can be solved largely if HSM is used here as a third predictor. HSM (as a third predictor) will enable shifting a rescaled version of the nearest cloud free Landsat-8 in time by a few days back or forth to match the revisit time of Sentinel-1. Accordingly, HSM will account for any moisture source that occurred between revisit times.
- Based on the above discussion, it can be concluded that the three approaches perform nearly equal in terms of accuracy but each has different sources of uncertainties and calibration requirements. They are recommended for usage after the necessary calibration of each. A switch between the three approaches can also be used (e.g., Landsat-8 based models can be excluded in cloudy cases). Finally, the three-predictors approach discussed in the point above may act as a strong candidate for the two-predictor approaches investigated in this paper. The current research opens the door to future investigations using such three predictors approach.

Research in Europe reported anomalous Sentinel-1 cases in very dry conditions where the backscattered energy anomalously decrases when adding moisture until a turning point where the relation becomes normal (backscatter increases with moisture). A significant number of studies explained this behaviour due to the contribution of the sub-surface backscattering in very dry conditions. On the other side, in semi-arid regions, measured data revealed another turning point that occurs in wet conditions, after which the backscatter anomalously decreases when adding moisture. The explanation here is certainly not related to the sub-surface contribution but it might be related to the smoothing effects of moisture at the surface, which reflects energy away from the radar antenna due to the incident angle. This effect will be strongly apparent inside Wadi areas where highly wet conditions can significantly smooth/liquefy the surface. The paper showed that the inclusion of a second predictor (as an anomaly detector) could solve this problem. This paper focuses mainly on applications requiring the highest possible spatial resolution and less temporal resolution (e.g., water demand and irrigation applications). For other applications such as rainfall-runoff modeling (whether offline or real-time), the methodology described in the paper can also be used but with different types of satellites that use the same mesoscale spatiotemporal resolution (i.e., MODIS). This is also recommended for future studies.

**Acknowledgment**

The authors are deeply grateful to the following organizations (in alphabetic order) for providing the data as well as for the technical support in dealing with the different data formats:

- The European Space Agency for providing Sentinel-1 data.

- The United States Geological Survey for providing Landsat-8 data.
- The Water Resources Research Institute in Egypt (WRRI) for providing the rain gauge data.

This research was funded by the Egyptian Academy of Scientific Research and Technology (ASRT) through the research project "Strategies for increasing the water use efficiency of semi-arid Mediterranean agro-silvopastoral systems under climate Change (FLUXMED)", which was awarded through a Water-JPI call. The Water-JPI program was launched in the framework of the European partnership Water4All.

**References**

[1] Liu, Y., Qian, J. and Yue, H., (2021). Combined Sentinel-1A with Sentinel-2A to Estimate Soil Moisture in Farmland. *IEEE J. Sel. Top. Appl. Earth Obs. Remote Sens*., Vol. 14, 1292-1310. https://doi.org/10.1109/JSTARS. 2020.3043628.

[2] Mohamed, E. S., Ali, A., El-Shirbeny, M., Abutaleb, K. and Shaddad, S. M., (2020). Mapping Soil Moisture and their Correlation with Crop Pattern Using Remotely Sensed Data in Arid Regions. *Egypt. J. Remote Sens. Sp. Sci.*, Vol. 23(3), 347-353. https://doi.org/10.10 16/j.ejrs .2019.04.003.

[3] Sutariya, S., Hirapara, A., Meherbanali, M., Tiwari, M. K., Singh, A. and Kalubarme, M., (2021). Soil Moisture Estimation using Sentinel-1 SAR Data and Land Surface Temperature in Panchmahal District, Gujarat State. *Int. J. Env. and Geoinformatics*, Vol. 8(1), 65-77. https://doi.org/10.30897/ijegeo. 7774 34.

[4] Youssef, N. M., El Moustafa, A. M., Gad, M. A. and Elleithy, D. M., (2022). Soil Moisture Estimation Using Land Surface Temperature in the Northwestern Coast of Egypt. *Int. Res. J. Eng. Technol.*, Vol. 9(12), 1560–1569. https://www.irjet.net/archives/V9/i12/IRJET-V9I12258.pdf.

[5] Hassaan, A. M., Belal, A. A., Hassan, M. A., Farag, F. M. and Mohamed, E. S., (2019). Potential of Thermal Remote Sensing Techniques in Monitoring Waterlogged Area Based on Surface Soil Moisture Retrieval. *J. African Earth Sci*., Vol. 155, 64-74. https://doi.org/10.1016/j.jafrearsci.2019.04.005

[6] Zeng, Y., Feng, Z. and Xiang, N., (2004). Assessment of Soil Moisture Using Landsat ETM+ temperature/Vegetation Index in Semiarid Environment. *International Geoscience and Remote Sensing Symposium (IGARSS)*, Vol. 6, 4306-4309. https://doi.org/10.1109/igarss.2004.1370089.

[7] Amazirh, A., Merlin, O., Er-Raki, S., Gao, Q., Rivalland, V., Malbeteau, Y., Khabba, S. and Escorihuela, M. J., (2018). Retrieving Surface Soil Moisture at High Spatiotemporal Resolution from a Synergy between Sentinel-1 Radar and Landsat Thermal Data: A Study Case Over Bare Soil. *Remote Sensing of Environment*, Vol. 211, 321-337. https://doi.org/10.1016/j.rse.2018.04.013.

[8] Zhuo, L. and Han, D., (2016). The Relevance of Soil Moisture by Remote Sensing and Hydrological Modelling. Procedia Engineering, Vol. 154, 1368-1375. https://doi.org/10.1016/j. proeng.2016.07.499.

[9] Thoma, D. P., Moran, M. S., Bryant, R., Rahman, M., Holifield-Collins, C. D., Skirvin, S., Sano, E. E. and Slocum, K., (2006). Comparison of Four Models to Determine Surface Soil Moisture from C-band Radar Imagery in a Sparsely Vegetated Semiarid Landscape. *Water Resour. Res*., Vol. 42(1). https://doi.org/10.1029/2004WR003905.

[10] Mirsoleimani, H. R., Sahebi, M. R., Baghdadi, N. and El Hajj, M., (2019). Bare Soil Surface Moisture Retrieval From Sentinel-1 SAR Data Based on the Calibrated IEM and Dubois Models Using Neural Networks. *Sensors.* Vol. 19(14). https://doi.org/10.3390/s19143209.

[11] Baghdadi, N., El Hajj, M. and Zribi, M., (2019). An Operational High-Resolution Soil Moisture Retrieval Algorithm Using Sentinel-1 Images. *Progress in Electromagnetics Research Symposium*, https://doi.10.1109/PIERS-Spring 46901.2019.9017477.

[12] Doubková, M., Van Dijk, A. I. J. M., Sabel, D., Wagner, W. and Blöschl, G., (2012). Evaluation of the Predicted Error of the Soil Moisture Retrieval from C-band SAR by Comparison Against Modeled Soil Moisture Estimates over Australia. *Remote Sens. Environ.*, 188-196. https://doi.org/10.1016/j .rse.2011.09.031.

[13] Şekertekin, A., Marangoz, A. M. and Abdikan, S., (2018). Soil Moisture Mapping Using Sentinel-1A Synthetic Aperture Radar Data. *Int. J. Environ. Geoinformatic*s, Vol. 5(2), 178-188. https://doi.org/10.30897/ijegeo.425 606.

[14] Chung, J., Lee, Y., Kim, J., Jung, C. and Kim, S., (2022). Soil Moisture Content Estimation Based on Sentinel-1 SAR Imagery Using an Artificial Neural Network and Hydrological Components. *Remote Sens.*, Vol. 14(3). https://

doi.org/ 10.3390/rs14030465.

[15] Bahar, E., (1981). Scattering Cross Sections for Composite Random Surfaces: Full Wave Analysis. *Radio Science*, Vol. 16(6), 1327-1335. https://doi.org/10.1029/RS016i006p01327.

[16] Fung, A. K., Liu, W. Y., Chen, K. S. and Tsay, M. K., (2002). An Improved IEM Model for Bistatic Scattering from Rough Surfaces. *J. Electromagn. Waves Appl.*, Vol. 16(5). 689-702.https://doi.org/10.1163/156939302X01119

[17] Wagner, W., Lindorfer, R., Melzer, T., Hahn, S., Bauer-Marschallinger, B., Morrison, K., Calvet, J. C., Hobbs, S., Quast, R., Greimeister-Pfeil, I. and Vreugdenhil, M., (2022). Widespread Occurrence of Anomalous C-band Backscatter Signals in Arid Environments Caused by Subsurface Scattering. *Remote Sensing of Environment*, Vol. 276. https://doi.org/10.1016/j.rse.2022.113025.

[18] Fascetti, F., Pierdicca, N., Pulvirenti, L., Crapolicchio, R. and Muñoz-Sabater, J., (2016). A Comparison of ASCAT and SMOS Soil Moisture Retrievals over Europe and Northern Africa from 2010 to 2013. *Int. J. Appl. Earth Obs. Geoinf.*, Vol. 45, 135-142. https://doi.org/10. 1016/j.jag.2015.09.008.

[19] Mousa, B. G. and Shu, H., (2020). Spatial Evaluation and Assimilation of SMAP, SMOS, and ASCAT Satellite Soil Moisture Products Over Africa Using Statistical Techniques. *Earth Sp. Sci.*, Vol. 7(1). https://doi.org/10.1029/ 2019EA000841.

[20] Zhang, R., Kim, S., Sharma, A. and Lakshmi, V., (2021). Identifying Relative Strengths of SMAP, SMOS-IC, and ASCAT to Capture Temporal Variability. *Remote Sens. Environ*., Vol. 252. https://doi.org/10.1016/j.rse.2020.112126.

[21] Abdallah, M., (2016). *Rainfall-runoff Model for Water Management in Wadi Systems Based on Hydropedological Studies*. Master's Thesis, Mediterranean Agronomic Institute of Bari, Italy.

[22] Abdelmaqsoud, M. (2021). Retrieving Soil Moisture Content by Using Satellite Data: A Case Study of Wadi Kharouba, Egypt. Master's Thesis, Mediterranean Agronomic Institute of Bari, Italy.

[23] Moawad, B. M., (2012). *Geoscience General Tool Package for ARCGIS 10.x.* Unpublished User Manual for Desert Encroachment in Central Asia – Quantification of Soil Biogenic Nitric Oxide Emissions by Ground- and Satellite-Based Methodologies (DEQNO). Department of Biogeochemistry, Max-Planck-Institut für Chemie, Mainz-Germany, 1-49.

[24] Jiménez-Munoz, J. C. and Sobrino, J. A., (2003). A Generalized Single-Channel Method for Retrieving Land Surface Temperature from Remote Sensing Data. *J. Geophys. Res. Atmos.*, https://doi.org/10.1029/2003jd003480.

[25] Potin, P., Rosich, B., Miranda, N., Grimont, P., Shurmer, I., O'Connell, A., Krassenburg, M. and Gratadour, J., (2019). Copernicus Sentinel-1 Constellation Mission Operations Status. *International Geoscience and Remote Sensing Symposium (IGARSS)*, 5385-5388. https://doi.org/10.1109/IGARSS.2019.8898949.

[26] Filipponi, F., (2019). Sentinel-1 GRD Preprocessing Workflow. Proceedings 3rd International Electronic Conference on Remote Sensing, 22 May–5 June 2019, Vol. 18(1). https://doi.org/10.3390/ecrs-3-06201.

[27] Park, J. W., Korosov, A. A., Babiker, M., Sandven, S. and Won, J. S., (2018). Efficient Thermal Noise Removal for Sentinel-1 TOPSAR Cross-Polarization Channel. *IEEE Trans. Geosci. Remote Sens.*,Vol. 56(3), 1555-1565. https://doi.org/10.1109/TGRS.2017.2765248.

[28] Chow, V. T., Maidment, D. R. and Mays, L. W., (1988). *Development of Hydrology*. [Online]. Available: https://wecivilengineers.files.wordpress.com/2017/10/applied-hydrology-ven-te-chow.pdf

[29] Awadallah, A. G., Saad, H., ElMoustafa, A. and Hassan, A. (2016). Reliability Assessment of Water Structures Subject to Data Scarcity using the SCS-CN Model. *Hydrological Sciences Journal*, Vol. 61(4), 696-710. https://doi.org/10.1080/02626667.2015.1027709.

[30] Gad, M. A., (2013). A Useful Automated Rainfall-Runoff Model for Engineering Applications in Semi-Arid Regions. *Comput. Geosci.*, Vol. 52, 443-452. https://doi.org/10.1016/ j.cageo.2012.09.023.

[31] Foda, R. F., Awadallah, A. G. and Gad, M. A., (2017). A Fast Semi-Distributed Rainfall-Runoff Model for Engineering Applications inArid and Semi-Arid Regions. *Water Resour. Manag.*, Vol. 31, 4941–4955. https://doi.org/10.1007/s11269-017-1787-2